

# An Analysis of Continuum Emission in NGC5331

Savannah Woods, Loreto Barcos-Muñoz, Devaky Kunneriath

## Abstract

We present an analysis of NGC5331, part of the Great Observatories All-Sky LIRG Survey (GOALS) and examine continuum emission obtained through the VLA, ALMA, Herschel, and Spitzer. Using flux measurements from aperture photometry, we model the Spectral Energy Distribution (SEDs) for a set of images tapered to  $\sim 1''$  and a set tapered to  $6''$ . We find the emission fits well the modeled power law for thermal and nonthermal emission. We find thermal fractions  $< 50\%$  in global measurements of the component galaxies, but at smaller scales 2 regions in the south are  $> 50\%$ . From the flux at 33 GHz, the Star Formation Rate (SFR) is found to be  $\sim 7 M_{\odot}/yr$  in the northern galaxy and  $\sim 30 M_{\odot}/yr$  for the southern galaxy. These values correlate well with the SFR derived from total infrared luminosity, matching within the range of the uncertainties considered. From this, we conclude that NGC5331 provides further confirmation of the radio-IR relationship for star formation.

## Introduction

Luminous Infra-Red Galaxies (LIRGS) are defined as having  $L_{IR} > 10^{11} L_{\odot}$ . These galaxies are very often members of mergers and interacting systems. These are of interest to astronomers studying the evolution of galaxies and star formation, and a collaborative group work on the Great Observatories All-sky LIRG Survey (GOALS) that compiles multiwavelength data from 200 U/LIRGs. Radio observations of these objects allow the study of dusty star forming regions that are obscured at optical wavelengths. The radio emission is caused by massive stars that experience a supernova and produce non thermal synchrotron radiation as well as the massive stars that help ionize the HII regions and emit free free thermal emission. Below 33 GHz the emission is generally dominated by nonthermal emission and in the approximate range of 33-100GHz the emission is dominated by thermal emission, at higher frequencies, thermal dust reradiation becomes the dominant emission mechanism. Stereotypically, the intense IR emission from LIRGS is from molecular gas rich mergers.

# Observations and Data Analysis

## Galaxy selection

The GOALS sample were originally members of the IRAS survey in 1986. Based on different characteristics they were chosen to be LIRGs if they had an infrared luminosity greater than  $10^{11} L_{\text{sun}}$ , and said to be Ultra Luminous Infrared Galaxies (ULIRGs) if their infrared luminosity surpassed  $10^{12} L_{\text{sun}}$ . The GOALS sample selected a group of about 180 LIRGs and 20 ULIRGs to compile multiwavelength data in order to create an in depth and far reaching survey of the properties of these bright objects. Many of the galaxies in GOALS share certain characteristics: being in an interacting system/merger, having spiral arms and bars, being dusty and optically thick at higher wavelengths but thin at radio and IR wavelengths, have small compact regions of gas and dust that ultimately become Star Forming (SF) regions.

NGC5331 was chosen for this analysis due to the availability of VLA, ALMA, Herschel, and Spitzer data. It is an interacting pair of spiral galaxies  $>150$  Mpc away from Earth. The system is likely in the early stages of a merger with clear northern and southern components. Figure 1 shows an HST image, notice the spatial extent of the spiral arms- the Northern galaxy's spiral arms have a physical extent similar to the South at this observed wavelength.

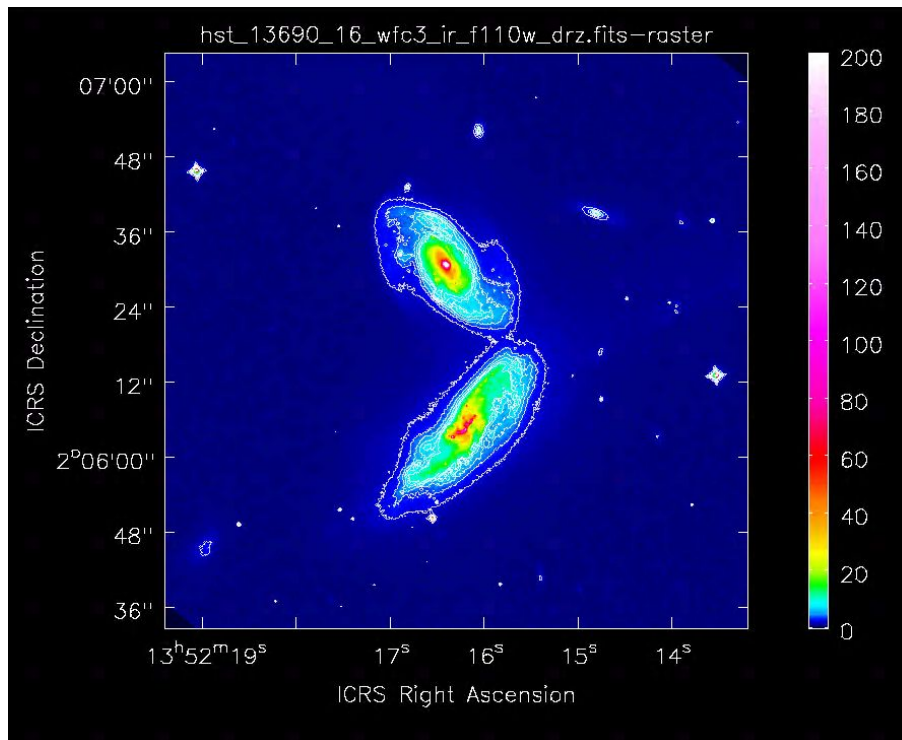


Figure 1) Hubble Space Telescope image of NGC5331 showing two interacting grand design spiral galaxies in NGC5331, white contours show emission that is 3, 5, and 7 times greater than the background noise level.

## VLA

The VLA data analyzed for this project was observed at S, Ku, and Ka bands or 3, 15, and 33GHz respectively. For each band, observations were taken in two different configurations: A with a maximum baseline of 36.4 km and C with a maximum baseline of 3.4 km.

A summary of the observation properties are given in table 1.

From here, the measurement sets were put through the CASA pipeline developed by ALMA, self calibrated and flagged. To create the images, the measurement sets for the different configurations were combined and the standard telean task in CASA was used; using robust value of 0.5.

Examples of final images are shown in Figure 2.

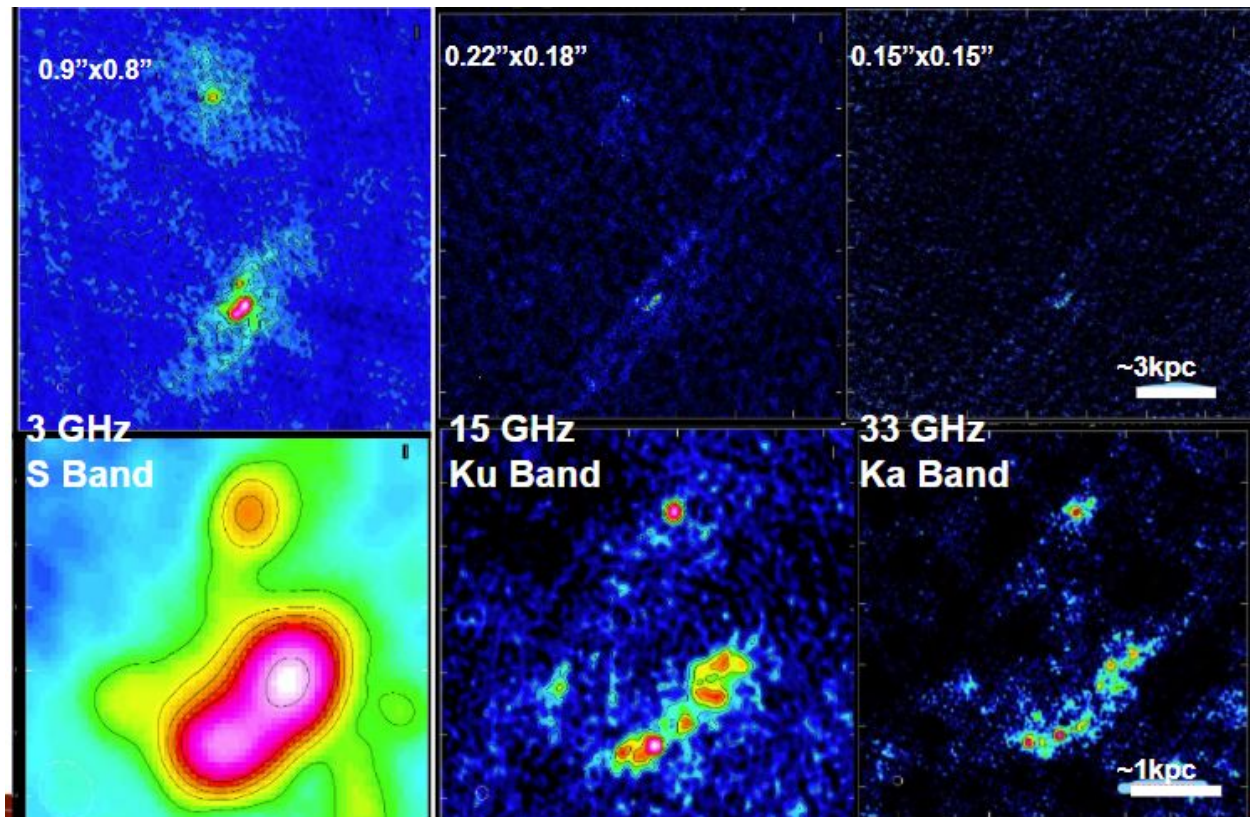


Figure 2) VLA images at 3,15,and 33 GHz. The top three panels show both the northern and southern galaxies while the bottom shows a magnified view of the southern galaxy.

# ALMA

The ALMA data used included two different windows in Band 3, centered around 93 and 104 GHz. Both extended and compact configurations were utilized. A summary of the observation's properties are given in table 1. When two configurations of data were available for a spectral window, they were combined and a standard clean task was run; using 0.5 for the robust parameter. An example of the final image product is shown in Figure 3.

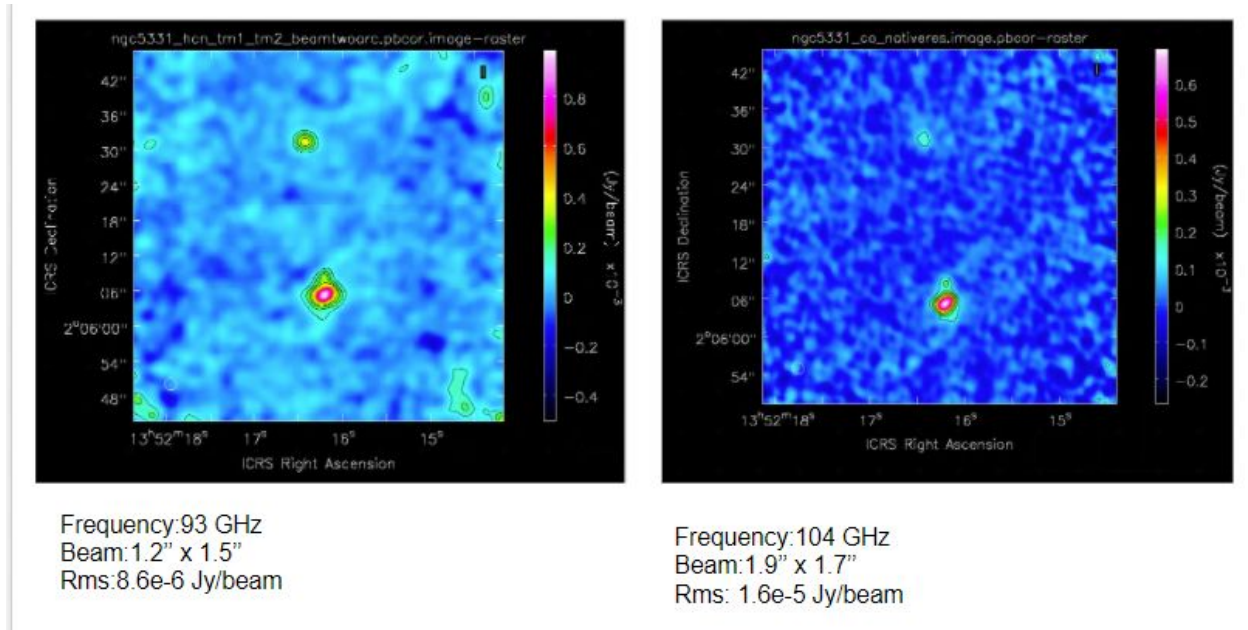


Figure 3) ALMA images from Band 3

Table 1 Observational Parameters						
Telescope	Observer	date	elapsed time (s)	frequency (GHz)	configuration	# of antennae
VLA	A Evans	04/09/2014	312	3	A	27
VLA	A Evans	11/15/2014	312	3	C	27
VLA	A Evans	04/22/2014	294	15	A	27
VLA	A Evans	11/08/2014	292	15	C	27
VLA	A Evans	04/18/2014	732	33	A	27
VLA	A Evans	03/04/2016	1233	33	C	27
ALMA	tmichiyama	10/06/2016	2.45E+07	93	extended	78
ALMA	tmichiyama	12/25/2016	1994.11	93	compact	46
ALMA	tmichiyama	12/23/2016	1240.94	104	compact	47

Table 1) Observation conditions

## Ancillary Data

IR data from the Herschel telescope and inspected, FITS images at 70, 100, 160, 250, 350, and 500 microns were examined. Since the IR images have a limiting angular resolution of only  $6''$ , the only structure to be seen was the distinction between the North and the South galaxies, at the highest wavelengths (350, 500 microns) the target could not even be separated into two components so the entire interacting system appeared as one smudge of light.

## Spitzer

One MIPS image from Spitzer was used at 24 microns. The benefit of adding this image was to sample a higher energy part of the IR regime and to help calculate total IR luminosities.

## Methods

### Creation of Beam Matched Image Sets

Wishing to compare fluxes as a function of frequency, images with compatible beam sizes needed to be created in order to compare accurately. Since we had data ranging from 3GHz all the way up to 24 microns, we found it most beneficial to examine different scales of structure by beam matching groups of images. To lower the angular resolution, the measurement sets were tapered using uv taper and setting the restoring beam constant when cleaning. The highest angular resolution images were beam matched to the 3GHz limiting resolution of about  $1''$ . These tapered VLA images would allow for SED analysis of individual clumps since the resolution was sufficient for this.

In order to study the global properties of these galaxies, a set of images were tapered to the limiting resolution of the IR data at  $6''$ . This image set would not provide any useful information on smaller structures, but would be able to compare fluxes across a wide range of wavelengths and to compare radio and IR fluxes directly.

### Region Photometry

To obtain relevant fluxes, circular apertures were drawn in CASA viewer and the regions assigned labels. Figure 4 shows the way the apertures were created for the  $\sim 1''$  resolution images, figure 5 shows the apertures drawn for the  $6''$  resolution images. The apertures were drawn based on the most extended emission at the 3sigma confidence level.

Across all images there are a few important trends to notice: the southern galaxy is significantly brighter, the northern galaxy appears compact, some extended spiral structure can be seen in the southern galaxy.

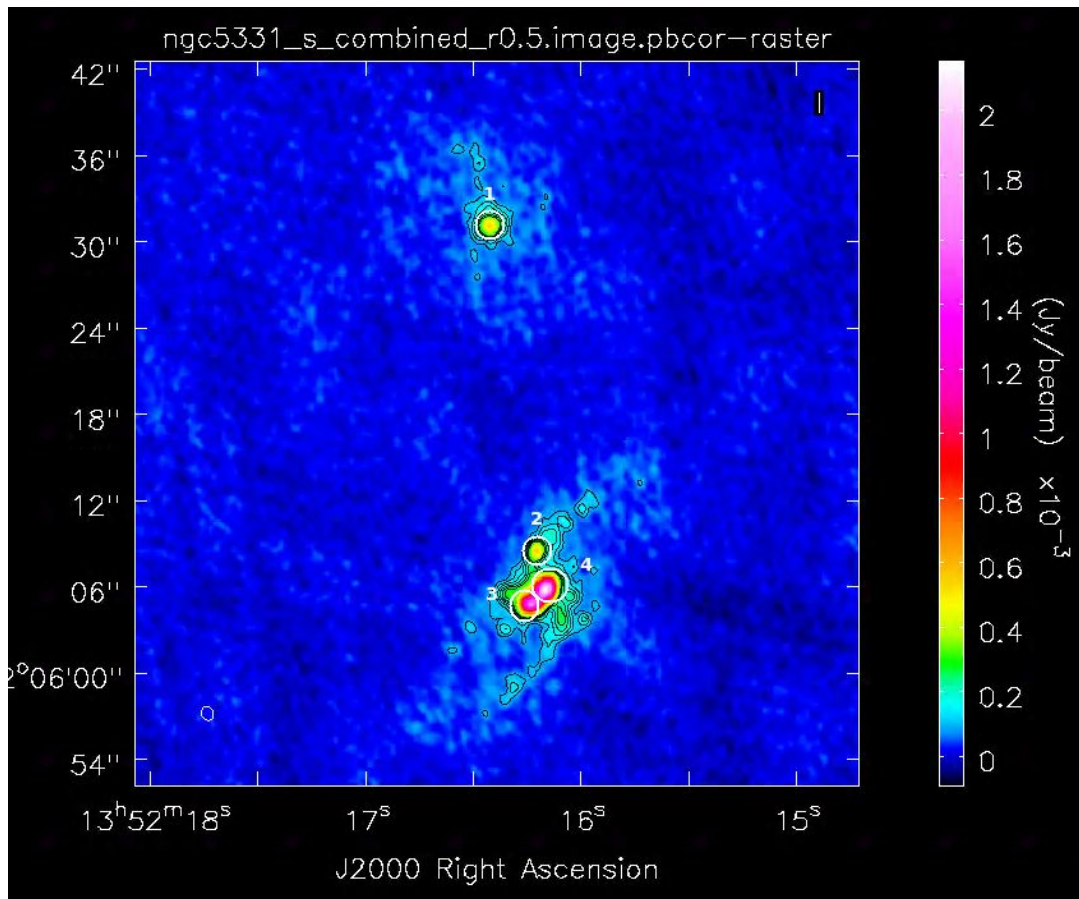


Figure 4) 3 GHz image with regions labeled with  $\sim 1''$  resolution; Regions 1, 2, and 3 have a diameter of  $2''$  and region 4 has diameter of  $2.4''$

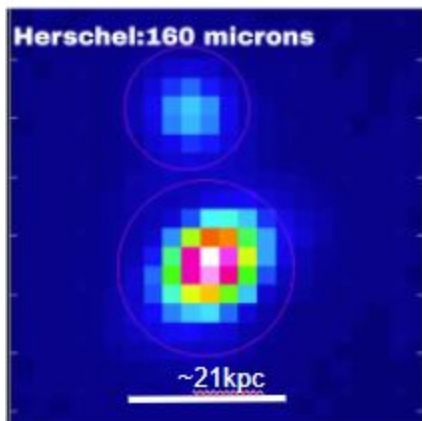


Figure 5) Herschel image depicting the circular apertures drawn; the Northern has a diameter of  $21''$  and the southern one has a diameter of  $30''$

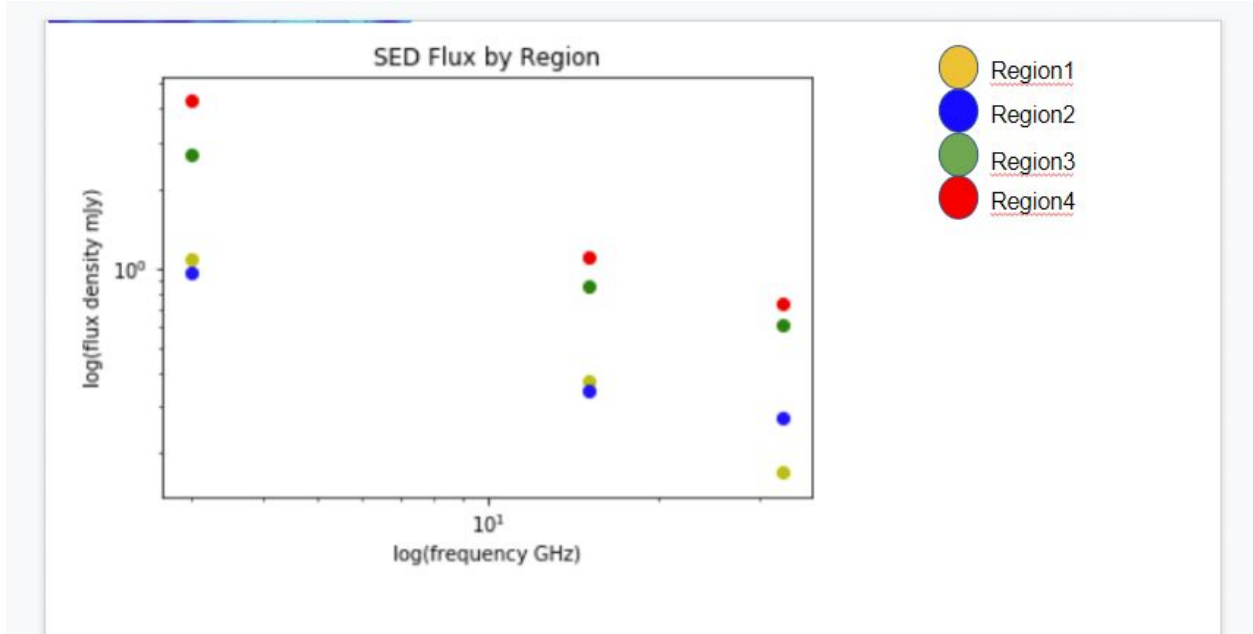


Figure 6) A graphical overview of the flux measurements of NGC5331 for the ~1'' images for the different regions

## Results and Discussion

From the aperture photometry, we derive spectral indices, model the SEDs, calculate thermal fractions and star formation rates.

### Spectral indices

The spectral index,  $\alpha$ , is a parameter that gives information about how quickly the intensity of emission changes with frequency.

$$\alpha = \frac{\log(S_1/S_2)}{\log(\nu_1/\nu_2)}$$

Average values for the spectral indices corresponding to thermal and non thermal emission are -0.1 and -0.85 respectively. Table 2 shows a sample experimental values that were calculated from the data.

NGC5331 North Galaxy			
	flux (Jy)	freq (Hz)	spectral index
VLA S	0.001089006	3000000000	
VLA Ku	0.000377	15000000000	-0.6590968418
VLA Ka	0.0001703	32999000000	-1.007935475

Table2) Flux measurements and  $\alpha$  for the northern galaxy using  $\sim 1''$  images using a  $2''$  aperture.

## SED modeling

Spectral Energy Distribution graphs were created for each region in which the fluxes were measured. Using a publicly available python library scipy, the task curvefit was used to fit the observational data with the functional form of the SED.

$$S_{\nu} = a * \nu^{-0.1} + b * \nu^{-0.85}$$

The free parameters that were fit were  $a$  and  $b$ , the coefficients determining the relative weight of the components of the power law. Constraints were set such that the parameters must be greater than 0 and the uncertainties were taken into account in the modeling. Two different types of uncertainty were considered and added in quadrature. The flux uncertainty was assumed to be 5% and the rms extended was calculated as in equation 3.

An example of the SED is shown in figure 7.

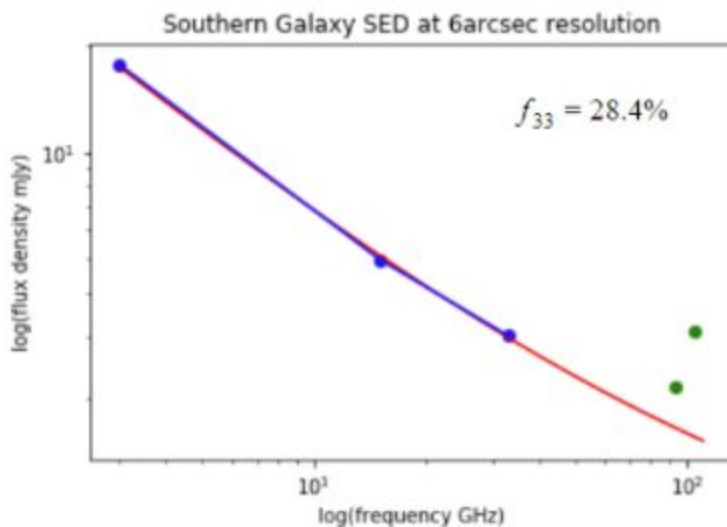


Figure 7) Spectral Energy Distribution for NGC5331 South from images at  $6''$  resolution, fluxes were measured in an aperture of  $30''$

Additionally, spectral index maps were created between the VLA images. We look to the maps to confirm the presence of overall patterns of emission distribution. Global measurements of the spectral indices can

be useful for broader average understanding. The maps provide information on how emission changes between frequencies and the location in the galaxy.

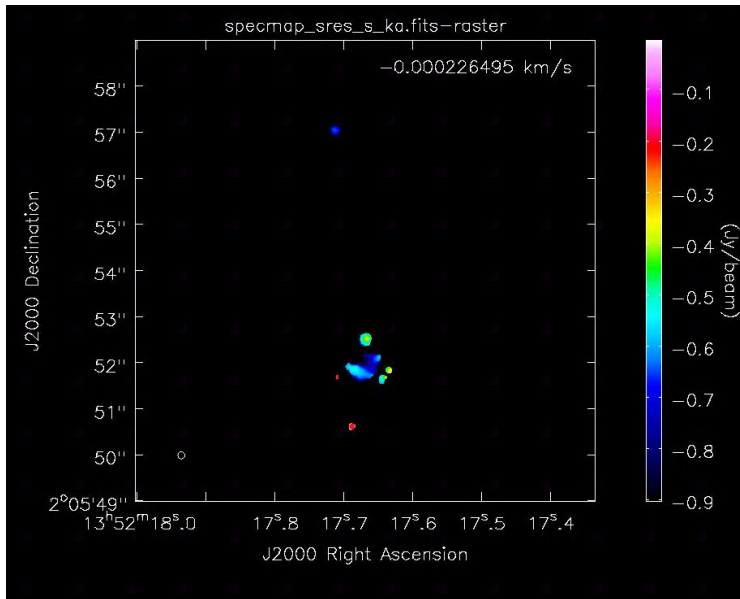


Figure 8) Spectral index map created from 3 and 33GHz images, note the steeper spectrum in the centers of both the north and south; this is congruent with other methods of analysis

## Thermal fractions

Thermal fractions are a way of determining how much of the total observed flux is originating from thermal processes.

It is important to compare the thermal fractions that are calculated here with average values for extranuclear star forming regions in LIRGS presented by Linden et al 2019 of ~65% at 33GHz.

~1" resolution	
Region	f_33 (%)
region1	20
region 2	63
region 3	50.9
region 4	28.2
6" resolution	
North	33.1
South	28.4

Table 3) thermal fractions at 33 GHz.

## Star formation rates and densities

Star formation rates are calculated using already established equations.

$$\left( \frac{\text{SFR}_\nu}{M_\odot \text{ yr}^{-1}} \right) = 10^{-27} \left[ 2.18 \left( \frac{T_e}{10^4 \text{ K}} \right)^{0.45} \left( \frac{\nu}{\text{GHz}} \right)^{-0.1} + \right. \\ \left. 15.1 \left( \frac{\nu}{\text{GHz}} \right)^{-\alpha_{\text{NT}}} \right]^{-1} \left( \frac{L_\nu}{\text{erg s}^{-1} \text{ Hz}^{-1}} \right).$$

**Murphy + 2012**

$$\left( \frac{\text{SFR}_{\text{IR}}^{\text{Avg.}}}{M_\odot \text{ yr}^{-1}} \right) = 3.15 \times 10^{-44} \left( \frac{L_{\text{IR}}}{\text{erg s}^{-1}} \right).$$

**Murphy 2012**

$$L_{\text{TIR}} = 2.176\nu L_{24} - 0.163\nu L_{70} + 1.739\nu L_{100}$$

Dale, priv. comm.

As seen in previous analyses of GOALS galaxies, the infrared SFR is compared to the SFR calculated at 33GHz. From the  $\sim 1''$  clump analysis we calculate SFR from 33GHz to be 1.7, 2.9, 6.0, and 7.2 solar masses per year for regions 1, 2, 3, and 4. Using the  $6''$  images, the SFR from 33GHz was 6.9 and 29.3 solar masses per year for the northern and southern galaxies. When calculating the SFR from the total infrared luminosity, we calculate 9.3 and 43.7 solar masses per year for the northern and southern galaxies. The SFR derived from 33 GHz and from the IR luminosity are consistent with the radio-IR correlation.

It is useful to know the location of the nuclei of the two galaxies so that any emission that could be coming from nuclear non-thermal activity could be identified and considered in the discussion of the SFR. It is possible that nuclear activity could cause a slight overrepresentation in the radio SFR as the nonthermal emission from the nucleus would not be a result of SF.

Region 1 is the northern nucleus by default, as it is the only part of the north that is observed. Also, the thermal fraction is lower than expected for an extranuclear star forming region, which adds to the determination that it is the nucleus of the north. In the southern galaxy, we have divided into 3 smaller regions. Region 2 is quite faint, so this is not believed to be the nucleus. However, it is not obvious if region 3 or 4 is more likely to be the nuclear region. On one hand, in the native resolution image at 15 GHz, region 3 seems to appear brighter and more compact than region 4; on the other hand the thermal fraction for region 4 is quite a bit smaller than region 3 which could indicate nuclear activity. Another, perhaps more likely explanation is that none of the clumps we see represent the true nucleus but are instead circumnuclear star forming regions and the inclination of the galaxy does not allow the true nucleus to be visible.

In the future, work will continue on enhancing the fortitude of the analysis methods, inspect brightness temperatures, and study moment zero maps for emission line data of CO. Moving forward, we intend to fill out our understanding of this system by ensuring accuracy and quality of the continuum emission data, look at the kinematics and dynamics of the molecular gas, and develop conclusions for the age of the galaxy, the depletion time of the gas clouds, and the star formation rate efficiency.

## References

Chu, Jason K., et al. “The Great Observatories All-Sky LIRG Survey: Herschel Image Atlas and Aperture Photometry.” *The Astrophysical Journal Supplement Series*, vol. 229, no. 2, 2017, p. 25., doi:10.3847/1538-4365/aa5d15.

Herrero-Illana, R., et al. “Molecular Gas and Dust Properties of Galaxies from the Great Observatories All-Sky LIRG Survey.” *Astronomy & Astrophysics*, vol. 628, 2019, doi:10.1051/0004-6361/201834088.

Linden, S. T., et al. “The Star Formation in Radio Survey: 3–33 GHz Imaging of Nearby Galaxy Nuclei and Extranuclear Star-Forming Regions.” *The Astrophysical Journal Supplement Series*, vol. 248, no. 2, 2020, p. 25., doi:10.3847/1538-4365/ab8a4d.

Murphy, E. J., et al. “The Star Formation in Radio Survey: Jansky Very Large Array 33 GHz Observations of Nearby Galaxy Nuclei and Extranuclear Star-Forming Regions.” *The Astrophysical Journal Supplement Series*, vol. 234, no. 2, 2018, p. 24., doi:10.3847/1538-4365/aa99d7.

Sanders, D. B., and I. F. Mirabel. “Luminous Infrared Galaxies.” *Annual Review of Astronomy and Astrophysics*, vol. 34, no. 1, 1996, pp. 749–792., doi:10.1146/annurev.astro.34.1.749.